# Hypocoordinated solids in particulate media

Thibault Bertrand,[1,4] Carl F. Schreck,[1,2] Corey S. O'Hern,[1,2,3,4] and Mark D. Shattuck[1,5]
[1]*Department of Mechanical Engineering & Materials Science, Yale University, New Haven, Connecticut 06520-8260, USA*
[2]*Department of Physics, Yale University, New Haven, Connecticut 06520-8120, USA*
[3]*Department of Applied Physics, Yale University, New Haven, Connecticut 06520-8120, USA*
[4]*Center for Research on Interface Structures and Phenomena, Yale University, New Haven, Connecticut 06520, USA*
[5]*Benjamin Levich Institute and Physics Department, The City College of the City University of New York, New York, New York 10031, USA*
(Received 1 July 2013; published 12 June 2014)

We propose a "phase diagram" for particulate systems with purely repulsive contact forces, such as granular media and colloids. We characterize two classes of behavior as a function of the input kinetic energy per degree of freedom $T_0$ and packing fraction deviation from jamming onset $\Delta\phi = \phi - \phi_J$ using simulations of frictionless disks. Isocoordinated solids (ICS) exist above jamming; they possess an average contact number equal to the isostatic value $z_{\rm iso}$. ICS display "strict" harmonic response, where the density of vibrational modes from the Fourier transform of the velocity autocorrelation function is a set of sharp peaks at eigenfrequencies $\omega_k^d$ of the dynamical matrix. In contrast, hypocoordinated solids (HCS) occur above and below jamming and possess fluctuating networks of interparticle contacts but do not undergo cage-breaking particle rearrangements. The density of vibrational frequencies for the HCS is not a collection of sharp peaks at $\omega_k^d$, but it does possess a common form over a range of $\Delta\phi$ and $T_0$.

DOI: 10.1103/PhysRevE.89.062203 PACS number(s): 45.70.−n, 63.50.−x, 64.70.pv

## I. INTRODUCTION

The vibrational response of conventional solids, such as metals, ceramics, and minerals, can be described by the harmonic approximation at sufficiently low temperatures compared to the melting points [1]. Nonlinearities stemming from weak structural disorder and the shape of the interaction potential explored at low temperatures can be treated as small perturbations [2]. Particulate systems, such as granular media [3] and colloids [4], can also exist in solidlike states in the limit of weak driving or thermal fluctuations. However, in contrast to molecular-scale solids, where interactions extend beyond one atomic diameter, the interactions in many particulate solids are purely repulsive and vanish when particles come out of contact. Even small changes in the contact network in purely repulsive particulate solids (both crystalline and disordered) can give rise to strong nonlinearities in the vibrational response [5–7]. This occurs whenever the number of instantaneous contacts between particles is less than the number of degrees of freedom in the system, which causes zero eigenvalues in the dynamical matrix. Such contact-breaking nonlinearities do not occur in conventional solids with interactions that extend well beyond a particle diameter [8], because there are significantly more interactions in these systems than degrees of freedom [9].

In spite of these nonlinearities, a major emphasis of the literature for jammed particle-based solids in the past decade has been to invoke the harmonic approximation for static packings to provide insight into structural relaxation of dense liquids near the glass transition [10,11]. However, one of the most obvious and important questions has been left unanswered: what is the *measured* response of static packings near jamming onset when they are subjected to vibrations? In this manuscript, we do not rely on the harmonic approximation to infer vibrational behavior. Instead, we measure directly the vibrations of model particulate systems as a function of the packing fraction deviation from jamming onset $\Delta\phi = \phi - \phi_J$ and input kinetic energy $T_0$.

We identify two classes of behavior in the $\Delta\phi$ and $T_0$ plane near jamming, as shown in Fig. 1: iso- and hypocoordinated solids (ICS and HCS), which are distinguished by the time-averaged contact number $\langle z\rangle$ and density of vibrational modes $D(\omega)$. For the ICS, with $\Delta\phi > \Delta\phi_c(T_0) > 0$, the contact network does not change from that at $T_0 = 0$, the contact number remains at the isostatic value, $\langle z\rangle = z_{\rm iso}$, and the vibrational response is harmonic, with strong peaks in the Fourier transform of the velocity autocorrelation function at the dynamical matrix eigenfrequencies. HCS occur both above and below $\phi_J$ [12] in the region defined by $\Delta\phi_+(T_0) > \Delta\phi > \Delta\phi_{cb}(T_0)$. In HCS, the network of interparticle contacts fluctuates with $\langle z\rangle/z_{\rm iso} < 1$, the vibrational response is strongly nonharmonic, and the form of $D(\omega)$ depends on the measurement method. In the regime $\Delta\phi < \Delta\phi_{cb}(T_0)$, cage-breaking particle rearrangements occur and $D(\omega)$ resembles that for dense liquids (DL).

## II. METHODS

We measure the vibrational response of mechanically stable (MS) packings of $N$ bidisperse frictionless disks with mass $m$ that interact via the pairwise purely repulsive potential

$$V(r_{ij}) = \frac{\epsilon}{2}\left(1 - \frac{r_{ij}}{\sigma_{ij}}\right)^2 \Theta\left(1 - \frac{r_{ij}}{\sigma_{ij}}\right), \qquad (1)$$

where $r_{ij}$ is the separation between disk centers, $\sigma_{ij} = (\sigma_i + \sigma_j)/2$ is the average disk diameter, $\epsilon$ is the energy scale of the repulsive interaction, and $\Theta(x)$ is the Heaviside step function. The bidisperse mixtures contained half-large and half-small disks by number with diameter ratio $r = \sigma_2/\sigma_1 = 1.4$. We focus on the $\Delta\phi \to 0$ limit, for which the MS packings possess the isostatic number of interparticle contacts $N_c^{\rm iso} = 2N - 1$, where $N = N' - N_r$ and $N$ is the number of particles after $N_r$ rattler particles with fewer than three contacts have been removed.

 

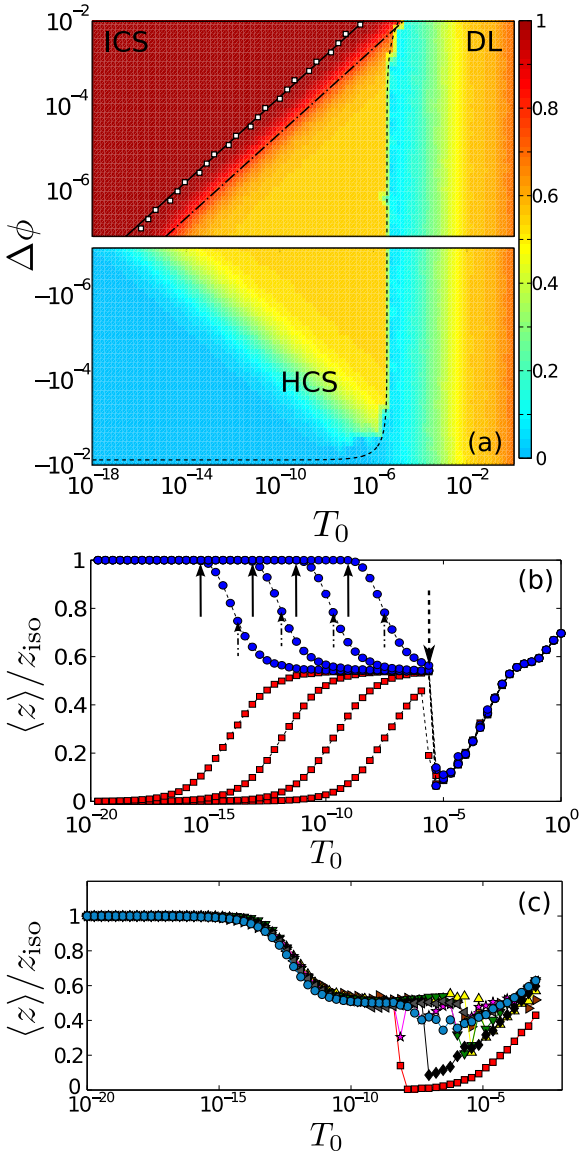


FIG. 1. (Color online) (a) Phase diagram for the vibrational response of MS packings versus $\Delta\phi$ and $T_0$, illustrated by heating and compressing (or decompressing) a single $N = 10$ packing at $\Delta\phi = 0$ and $T_0 = 0$ with a typical cage-breaking rearrangement temperature $T_{cb}$. The shading gives the time-averaged contact number $\langle z\rangle/z_{\rm iso}$. For $0 < \Delta\phi < \Delta\phi_c(T_0)$ (data and scaling curve given by open squares and solid line), the contact network for the ICS does not change from that at $T_0 = 0$ and the vibrational response is strictly harmonic. The midpoint $T_0$ at which $\langle z\rangle/z_{\rm iso}$ crosses over from 1 to 0.5 defines the boundary $\Delta\phi_+(T_0)$ (dot-dashed line with slope 0.5). In the HCS, the contact network fluctuates with $\langle z\rangle/z_{\rm iso} < 1$, but there are no particle rearrangements as in the DL regime with $\Delta\phi < \Delta\phi_{cb}(T_0)$ (dashed line). (b) $\langle z\rangle/z_{\rm iso}$ versus $T_0$ for a typical $N = 10$ packing compressed (decompressed) to $\Delta\phi = \pm 10^{-7}$, $\pm 10^{-6}$, $\pm 2\times 10^{-5}$, and $\pm 2 \times 10^{-4}$ (circles and squares) from left to right. The solid, dot-dashed, and dashed arrows indicate $\Delta\phi_c(T_0)$, $\Delta\phi_+(T_0)$, and $\Delta\phi_{cb}(T_0)$. (c) Time-averaged $\langle z\rangle/z_{\rm iso}$ versus $T_0$ for typical MS packings compressed to $\Delta\phi = 10^{-6}$ at several system sizes: $N = 10$ (rightward triangles), 16 (squares), 32 (upward triangles), 64 (downward triangles), 128 (stars), 256 (diamonds), 512 (leftward triangles), and 1024 (circles). Note that there is weak system-size dependence for $\langle z\rangle/z_{\rm iso}$ prior to particle rearrangement events.

We generate MS packings at $\Delta\phi_0 = 10^{-8}$ using the successive compression and decompression protocol described previously [13] for system sizes from $N = 10$–1024. Each packing was then decompressed or overcompressed in a single step to $-10^{-2} \leqslant \Delta\phi \leqslant 10^{-2}$ followed by conjugate gradient energy minimization to the configuration $\vec{R}^0 = \{x_1^0, y_1^0, \ldots, x_N^0, y_N^0\}$.

We perturbed each system at $\vec{R}^0$ by exciting equal kinetic energy in each mode [14]. We selected initial particle velocities $\vec{v} = \{v_{xi}, v_{yi}, \ldots, v_{xN}, v_{yN}\}$ according to

$$v_n = \delta \sum_{k=1}^{2N-2} e_n^k, \tag{2}$$

where $\hat{e}^k$ are the $2N-2$ eigenvectors (corresponding to the nonzero eigenvalues) of the dynamical matrix [15] evaluated at $\vec{R}^0$, $(\hat{e}^k)^2 = 1$, and $\delta$ is chosen so that $T_0 = \epsilon^{-1}\sum_i \frac{1}{2} m v_i^2/(2N-2)$ is in the range $10^{-20} \leqslant T_0 \leqslant 10^{-1}$. We then integrated Newton's equations of motion at constant total energy and area in a square box using the velocity Verlet algorithm with time step $\Delta t = 1/(400\pi)\sigma_1\sqrt{m/\epsilon}$. We first ran the constant energy simulations for $10^3$ oscillations of the lowest dynamical matrix eigenfrequency $\omega_1^d$ and then quantified fluctuations in particle positions over the next $10^3$ periods (or $10^3$ particle collisions for systems below jamming).

In the strict harmonic regime, the time-dependent particle positions are described by

$$R_n(t) = R_n^0 + \sum_{k=1}^{2N-2} A_k e_n^k \sin\left(\omega_k^d t + \psi_k\right), \tag{3}$$

where $A_k$ and $\psi_k$ are the time-independent amplitudes and phases of the normal modes $\hat{e}_k$ with eigenfrequency $\omega_k^d$ from the dynamical matrix. We employed two additional methods to measure the vibrational response as a function of $\Delta\phi$ and $T_0$. We calculated the Fourier transform of the normalized velocity autocorrelation function to quantify the density of vibrational modes [16]

$$D(\omega^v) = \int_0^\infty dt \frac{\langle \vec{v}(t_0+t)\cdot\vec{v}(t_0)\rangle}{\langle \vec{v}(t_0)\cdot\vec{v}(t_0)\rangle} e^{i\omega^v t}, \tag{4}$$

where $\langle . \rangle$ indicate averages over all particles and time origins $t_0$. We also measured the eigenvalue spectrum of $S = VC^{-1}$ [which equals the dynamical matrix $M$, provided Eq. (3) holds], where $V_{ij} = \langle v_i v_j\rangle$ are the elements of the velocity matrix,

$$C_{ij} = \left\langle \left(R_i - R_i^0\right)\left(R_j - R_j^0\right)\right\rangle \tag{5}$$

are the elements of the displacement correlation matrix [17], and angle brackets indicate averages over time. Vibrational frequencies $\omega_k^s = \sqrt{s_k}$ can be obtained from the eigenvalues of $S$. The binned versions of the density of vibrational frequencies are given by $D(\omega^{s,d}) = [\mathcal{N}(\omega^{s,d} + \Delta\omega^{s,d}) - \mathcal{N}(\omega^{s,d})]/[\mathcal{N}(\infty)\Delta\omega^{s,d}]$, where $N(\omega)$ is the number of frequencies less than $\omega$. $D(\omega^d)$, $D(\omega^v)$, and $D(\omega^s)$ are normalized so that $\int_0^\infty d\omega D(\omega) = 1$.

## III. RESULTS

In Fig. 2, we show the density of vibrational frequencies $D(\omega^v)$ obtained from the Fourier transform of the velocity

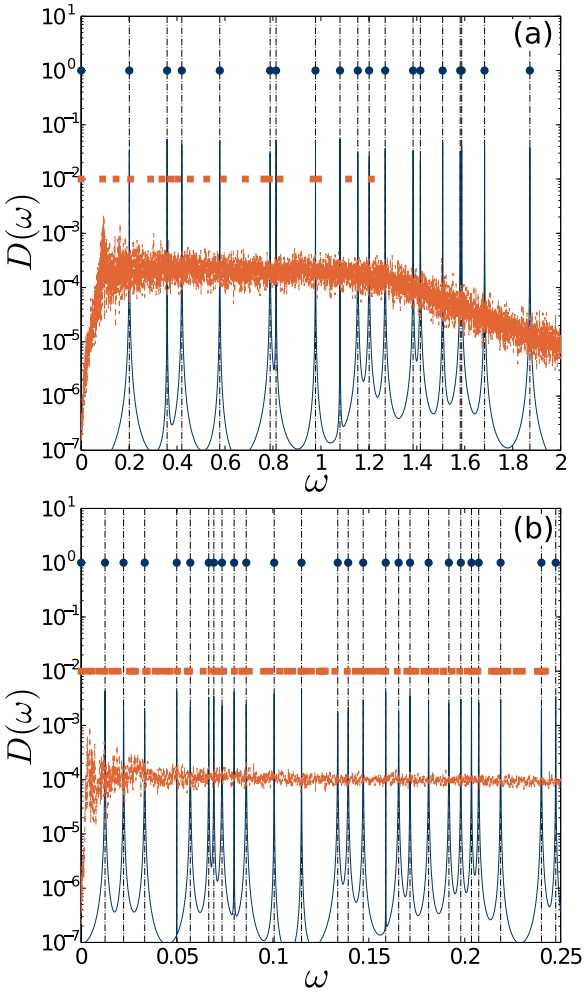


FIG. 2. (Color online) Comparison of portions of the density of vibrational frequencies $D(\omega)$ from the Fourier transform of the velocity autocorrelation function (lines) and associated with the dynamical (vertical dot-dashed lines) and displacement correlation matrices (symbols) in the ICS regime at $\Delta\phi = 2\times10^{-7}$ and $T_0 = 4\times10^{-19}$ (blue solid lines and circles) and HCS at $\Delta\phi = 2\times10^{-7}$ and $T_0 = 2\times10^{-11}$ (orange dashed lines and squares) for typical MS packings with (a) $N = 10$ and (b) 128. See Appendix D for a discussion of the finite widths of the distinct peaks in $D(\omega^v)$ in the ICS.

autocorrelation function for MS packings at $\Delta\phi > 0$, two $T_0$, and two system sizes. For sufficiently low $T_0$ in the ICS, the system displays strict harmonic response. The fluctuating particle positions are given by Eq. (3), and $D(\omega^v) = \sum_{k=1,2N-2}\delta(\omega^v - \omega_k^{d,s})$ is a set of $2N-2$ $\delta$-functions at frequencies that correspond to the eigenfrequencies of the dynamical and displacement correlation matrices. (In Appendix D, we show that $D(\omega^v)$ in the ICS matches a discrete Fourier transform of a harmonic function for several time resolutions.) For larger $T_0$, the instantaneous contact network deviates from that at $T_0 = 0$, and the vibrational response is no longer strictly harmonic. In the HCS regime, we find that $\omega_k^s < \omega_k^d$ (assuming the eigenvalues are sorted from smallest to largest), $D(\omega^v)$ becomes broad without strong peaks, and $D(\omega^v)$, $D(\omega^s)$, and $D(\omega^d)$ do not match. The same behavior is shown for both $N = 10$ and 128.

In Fig. 3(a), we show the dependence of the frequencies $\omega_k^s$ associated with the displacement correlation matrix versus $T_0$ and $\Delta\phi$ for a typical MS packing above and below $\phi_J$. For $\Delta\phi > 0$, $\omega_k^s = \omega_k^d$ for all $k$ in the ICS when $T_0 < T_c(\Delta\phi)$. For $T_0 > T_c(\Delta\phi)$ and $\Delta\phi > 0$, the frequencies $\omega_k^s$ first decrease with $T_0$ and then each reaches a $k$-dependent plateau value $\omega_k^* < \omega_k^d$ that persists for more than 6 orders of magnitude (at $\Delta\phi = 10^{-6}$). The plateau ends abruptly after a particle rearrangement occurs at $T_{cb}(\Delta\phi)$. The range of temperatures $T_0$ over which the plateau in frequency persists and $T_{cb}$ at which particle rearrangements occur varies strongly from one MS packing to another, as shown in Appendix C. Cage-breaking rearrangements were identified by comparing the particle positions for energy-minimized configurations $\vec{R}^{\min}$ originally at $T_0 > 0$ to those for the MS packing $\vec{R}^0$ at $T_0 = 0$. For $T_0 < T_{cb}(\Delta\phi)$, the distribution $P(\Delta R)$ of configurational distances $\Delta R = \sqrt{(2N)^{-1}\sum_{i=1}^{N}[(x_i^{\min} - x_i^0)^2 + (y_i^{\min} - y_i^0)^2]}$ [18] has a strong peak at small $\Delta R/\sigma_1 \sim 10^{-7}$ that corresponds to the precision of the particle positions after energy minimization. For both $\Delta\phi > 0$ and $\Delta\phi < 0$, $P(\Delta R)$ is bimodal for $T \gtrsim T_{cb}(\Delta\phi)$, with an additional well-separated peak at larger $\Delta R$ from cage-breaking particle rearrangements (see Appendix A). Note that after the system rearranges, the packing fraction at jamming onset shifts to $\phi_J' > \phi_J$, and thus the time-averaged contact number $\langle z\rangle$ drops precipitously at $T_{cb}$ (Fig. 1). After a rearrangement, the system can again be described by the phase diagram in Fig. 1 with $\Delta\phi = \phi - \phi_J'$.

For $\Delta\phi \leqslant 0$, there is no strict harmonic vibrational response regime. We find that the frequencies $\omega_k^s$ increase from zero at $T_0 = 0$ and reach the same $k$-dependent plateau values $\omega_k^*$ as those for $\Delta\phi > 0$ [19]. These results point to a robust set of frequencies (distinct from $\omega_k^d$) in HCS, where the contact network fluctuates, but the average contact number remains constant over a wide range of $T_0$ at $\langle z\rangle/z_{\rm iso} \approx 0.5$ [Figs. 1(b) and 1(c)]. We show similar results for crystalline disk packings with purely repulsive contact interactions in Appendix B.

Motivated by the behavior in the regime $\Delta\phi < 0$, for which the frequencies $\omega_k^s \sim \sqrt{T_0}/l_c(\Delta\phi)$ scale as the ratio of the velocity between interparticle collisions and typical cage size and then reach a plateau $\omega_k^*$ at large $T_0$, we propose the scaling function

$$\omega_k^s = \omega_k^*\left(1 + \frac{l_c(\Delta\phi)}{\sqrt{T_0}}\right)^{-1}, \tag{6}$$

where $l_c$ is measured in units of $\sigma_1$. In Fig. 3(b), we show least-squares fits of the maximum frequency associated with the displacement correlation matrix $\omega_m^s$ versus $T_0$ to Eq. (6) for logarithmically spaced packing fraction deviations below jamming in the range $10^{-7} \leqslant |\Delta\phi| \leqslant 10^{-2}$, all generated from the same $N = 10$ MS packing. (Similar quality fits are found for all lower frequencies.) Above jamming, $\omega_k^s$ interpolates between $\omega_k^d$ at $T_0 = 0$ and $\omega_k^*$ at large $T_0$. The generalized logistic function,

$$\omega_k^s(T_0) = \omega_k^d + \frac{\omega_k^* - \omega_k^d}{\left(1 + l_c(\Delta\phi)/T_0^{\alpha}\right)^{\nu}}, \tag{7}$$

which allows variations of the slope of $\omega_k^s(T_0)$ in the crossover region, is able to recapitulate $\omega_m^s$ below and above jamming

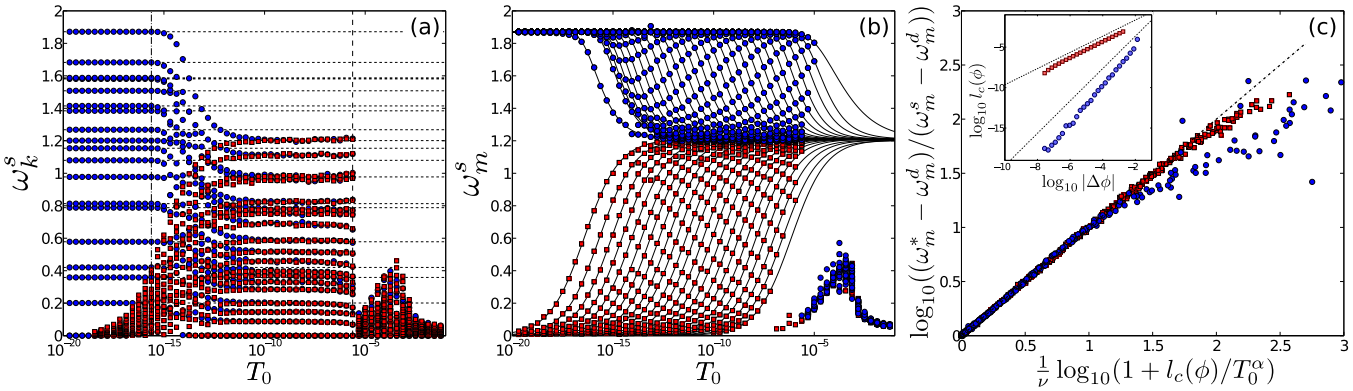


FIG. 3. (Color online) (a) The $2N-2$ frequencies $\omega_k^s$ associated with the displacement correlation matrix versus $T_0$ for a typical $N=10$ packing compressed to $\Delta\phi = 10^{-6}$ (blue circles) or decompressed to $-10^{-6}$ (red squares). The vertical dot-dashed and dashed lines indicate for $\Delta\phi = 10^{-6}$ the $T_c$ where the contact network first differs from that at $T_0 = 0$ and $T_{cb}$ where the energy-minimized configurations differ from that at $T_0 = 0$. The horizontal dashed lines show the dynamical matrix eigenfrequencies. (b) The maximum frequency $\omega_m^s = \max_k \omega_k^s$ versus $T_0$ for 28 logarithmically spaced packing fraction deviations $10^{-7} \leqslant |\Delta\phi| \leqslant 10^{-2}$ above and below jamming generated from the same $N=10$ packing in (a). The solid lines are fits of $\omega_m^s(T_0)$ to Eq. (7). (c) Scaled $\omega_m^s$ versus $T_0$. The inset shows $l_c$ versus $|\Delta\phi|$ above and below jamming. The dashed and dotted lines have slopes 1 and 2.

[Fig. 3(b)]. Below jamming, the best fits give $\alpha = 0.5$ and $\nu = 1$, i.e., Eq. (6). Above jamming, $\alpha \sim 0.6$ and $\nu \approx 0.25 l_c^{-1/2}$ over a wide range of $\Delta\phi$. In Fig. 3(c), we show that Eq. (7) collapses $\omega_m^s$ from (b) with some deviation at small $T_0$ above jamming (caused by numerical accuracy when $\omega_m^s \approx \omega_m^d$). In the inset to (c), we show that the generalized cage size scales as $l_c \sim \Delta\phi$ below and $\sim (\Delta\phi)^\lambda$ with $\lambda \gtrsim 2$ above jamming.

We summarize our results for the measured vibrational response of MS packings in the "phase diagram" in Fig. 1. For $\Delta\phi > \Delta\phi_c(T_0) \sim N^\beta \sqrt{T_0}/A$ [5], where $A \approx 0.5$ and $\beta \approx 0.85$, the contact network does not change from that at $T_0 = 0$. In the ICS, $\langle z \rangle = z_{\rm iso}$, the vibrational response is strictly harmonic, and the density of vibrational modes $D(\omega^v) = D(\omega^s) = D(\omega^d)$ [Figs. 4(a) and 4(b)]. Note that the size of the ICS decreases and the transition region between ICS and HCS widens with increasing $N$. In Fig. 1, we show that the midpoints of the crossovers in $\langle z \rangle / z_{\rm iso}$ from 1 to 0.5, which define $\Delta\phi_+(T_0)$, scale as $\sqrt{T_0}$. Assuming that the effective particle diameter shrinks with $\sqrt{T_0}$, we obtain an estimate for the shift in $\phi_J$ induced by thermal fluctuations [16,20–22]:

$$\Delta\phi_s(T_0) = \phi_J \left( \frac{1}{(1 - \sqrt{2T_0})^2} - 1 \right). \tag{8}$$

We find that near $\Delta\phi_s \sim \Delta\phi_+$ an extensive number of changes in the contact network from that at $T_0 = 0$ has occurred [7]. Similarly, for $\Delta\phi < 0$, an extensive number of "time-averaged" contacts has formed when $\Delta\phi > \Delta\phi_-$, and $\Delta\phi_-$ also scales as $\sqrt{T_0}$. However, we do not distinguish between regimes when crossing this boundary, because we can rescale the density of vibrational frequencies $D(\omega^s)$ from the displacement matrix for all systems with $\Delta\phi_+(T_0) > \Delta\phi > \Delta\phi_{cb}(T_0)$ onto a master curve [Fig. 4(c)].

In Figs. 4(a) and 4(b), we show the densities of vibrational frequencies $D(\omega^s)$ and $D(\omega^v)$ at $\Delta\phi = 10^{-6}$ for increasing $T_0$ from ICS to HCS. The density of vibrational frequencies begins to deviate strongly from the harmonic approximation when entering HCS [inset to Fig. 4(b)]. In HCS, the densities of vibrational frequencies display scaling forms, but

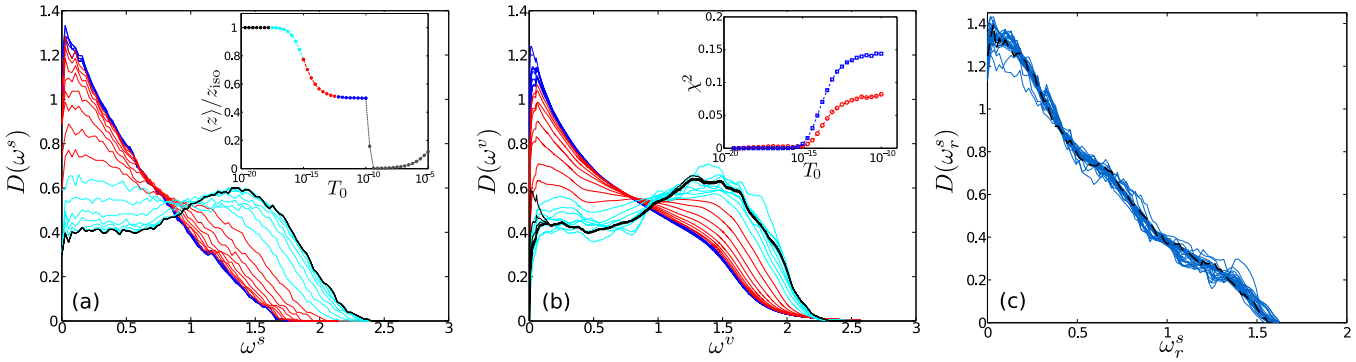


FIG. 4. (Color online) (a) $D(\omega^s)$ from the eigenvalues of the displacement matrix and (b) $D(\omega^v)$ from the Fourier transform of the velocity autocorrelation function for a typical $N = 128$ MS packing compressed to $\Delta\phi = 10^{-6}$. The line shadings in (a) and (b) indicate the time-averaged $\langle z \rangle / z_{\rm iso}$ and $T_0$ in the inset to (a) for the same packing. The inset to (b) shows the squared distance $\chi^2$ between the density of vibrational frequencies at a given temperature and that at $T_0 = 0$ for $D(\omega^s)$ (squares) and $D(\omega^v)$ (circles). (c) $D(\omega_r^s)$ (thin lines) for $N = 128$ obtained by rescaling the frequencies $\omega^s$ according to Eq. (6) to $T_0^* < T_{cb}$ for systems in HCS at $\Delta\phi = -10^{-7}$. The thick dashed line is the non-rescaled $D(\omega^s)$ at $T_0^*$.

$D(\omega^s) \neq D(\omega^v)$, e.g., $D(\omega^s)$ possesses a stronger peak at low frequencies and opposite curvature at high frequencies. In the transition regime, $\Delta\phi_c(T_0) < \Delta\phi < \Delta\phi_+(T_0)$, $D(\omega)$ varies continuously between that for ICS and HCS.

## IV. CONCLUSIONS

We emphasize that particulate systems over most of the $\Delta\phi$ and $T_0$ plane near jamming do not display strict harmonic vibrational response, i.e., $D(\omega^v)$ is broad, not a set of discrete, sharp peaks at the dynamical matrix eigenfrequencies $\omega_k^d$, and differs from other measures of the vibrational response. This implies that when particulate systems are excited by a single mode $\omega_k^d$, the response rapidly spreads to a broad spectrum of other modes. This result has important consequences for acoustic transmission [23] and thermal transport [24] in jammed solids. However, there is a wide swath of parameter space (corresponding to HCS) where the frequencies $\omega^s$ or $\omega^v$ can be rescaled such that $D(\omega^{s,v})$ separately obeys master curves. $D(\omega^{s,v})$ in this regime differs from $D(\omega^d)$ for $\Delta\phi > 0$ at $T_0 = 0$ and from $D(\omega)$ for dense liquids. In future work, we will measure the specific heat, thermal conductivity, quality factor, and other macroscopic physical quantities in the ICS and HCS regions.

## ACKNOWLEDGMENTS

We acknowledge support from the National Science Foundation (NSF), Grant No. CBET-0968013 (M.S.), the Defense Threat Reduction Agency, Grant No. 1-10-1-0021 (C.O. and T.B.), and seed funding from the NSF MRSEC, Grant No. DMR-1119826 (C.O. and T.B.).

## APPENDIX A: BOUNDARIES OF THE "PHASE DIAGRAM"

In this Appendix, we provide details concerning the definitions of the boundaries for the phase diagram in Fig. 1(a) that delineate the ICS, HCS, and DL regimes as a function of $\Delta\phi$ and $T_0$. In Fig. 5, we show the probability to undergo a cage-breaking particle rearrangement along with the boundaries of the phase diagram for the $N = 10$ packing in Figs. 1(a) and 1(b). We find that for $\phi > \phi_{cb}(T_0)$ there are no rearrangements over the course of the simulations. However, note that the boundary $\phi_{cb}(T_0)$ will vary with the total time of the simulation, i.e., particle rearrangements will occur at progressively lower $T_0$ and larger $\Delta\phi$ as the total time of the simulation is increased. After a particle rearrangement, the system will exist in the basin of a new static packing with $\phi_J' > \phi_J$; however, the system can still be described by the phase diagram in Fig. 1, except $\Delta\phi$ is given by $\phi - \phi_J'$.

In Fig. 6, we show the probability for obtaining separation $\Delta R$ in configuration space between the packing at $\Delta\phi$ and $T_0 = 0$ and an energy-minimized configuration at $\Delta\phi$ originally heated to $T_0$ for a system with $N = 10$. For $\Delta\phi > \Delta\phi_{cb}(T_0) > 0$, we find a strong peak for $\Delta R < 10^{-6}$, which indicates that the heated configurations have not undergone particle rearrangements and the small nonzero $\Delta R$ gives the resolution of the energy minimization. When $T_0$ increases above that required for cage-breaking particle rearrangements at a given $\Delta\phi$, another strong peak forms for $\Delta R > 10^{-1}$. For $\Delta\phi < 0$, the peak at small $\Delta R$ for systems that have

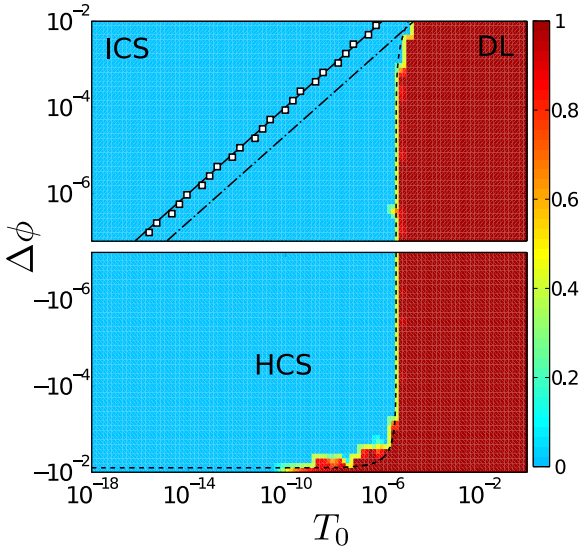


FIG. 5. (Color online) Phase diagram showing the ICS, HCS, and DL regimes in the $\Delta\phi$ and $T_0$ plane for a typical $N = 10$ packing [cf. Fig. 1(a) in the main text]. The shading shows the probability to undergo a cage-breaking particle rearrangement at each $\Delta\phi$ and $T_0$.

not undergone cage-breaking rearrangements is spread over several orders of magnitude, but is still well-separated from the large $\Delta R$ peak. Thus, before cage-breaking particle rearrangements, the systems are localized near their zero-temperature configurations.

Here we also provide a justification for the boundary $\Delta\phi_s$ [Eq. (8)] that separates the ICS and HCS regimes. In Fig. 7, we show a schematic that illustrates a disk packing undergoing

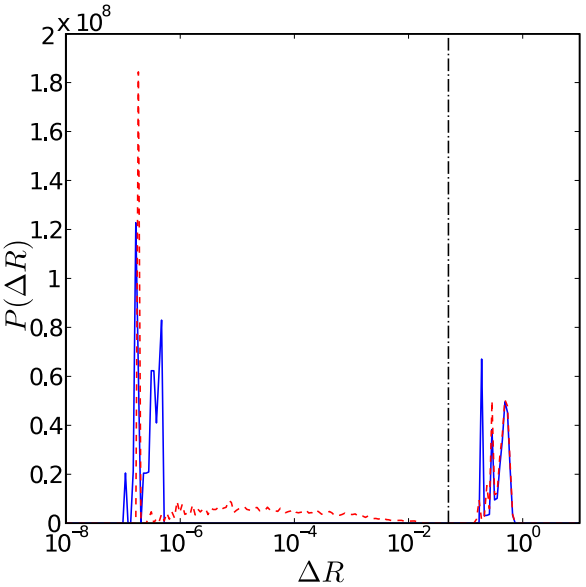


FIG. 6. (Color online) The probability $P(\Delta R)$ for obtaining separation $\Delta R$ in configuration space between the zero-temperature configuration at $\Delta\phi$ and configurations that have been thermally quenched from $T_0$ to zero temperature for $N = 10$ and $\Delta\phi = 10^{-4}$ (blue solid line) and $-10^{-4}$ (red dashed line). The vertical dot-dashed line indicates the threshold $\Delta R_c = 0.05$, above which we consider that the system has rearranged.

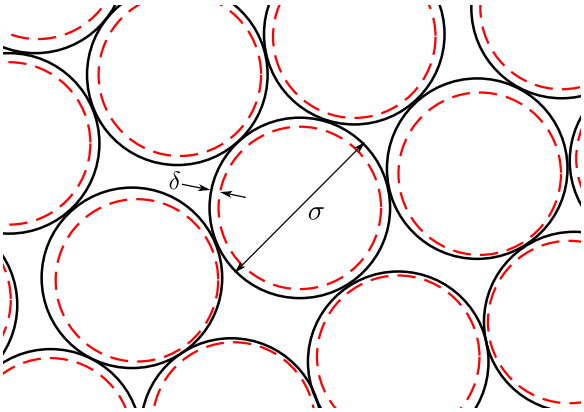


FIG. 7. (Color online) Illustration of a packing of disks with diameter $\sigma$ that is undergoing thermal fluctuations that give rise to average particle overlaps of size $\delta$. The dashed particle outlines indicate position fluctuations at temperature $T_0$.

thermal fluctuations. We consider a system of $N$ thermally fluctuating disks with diameter $\sigma$ that interact via purely repulsive linear spring potentials [Eq. (1)] at temperature

$$T_0 = \frac{\epsilon}{2}\left(\frac{\delta}{\sigma}\right)^2, \tag{A1}$$

where the average overlap between particles scales as

$$\delta \sim \sqrt{\frac{2T_0}{\epsilon}}\sigma. \tag{A2}$$

Since each disk can fluctuate a typical distance $\delta$ at temperature $T_0 > 0$, the effective diameter of each disk is reduced by $\delta$, and $\sigma_s = \sigma - \delta$. We can relate the effective jammed packing fraction $\phi_s(T_0)$ at $T_0$ to the jammed packing fraction $\phi_J$ at $T_0 = 0$:

$$\phi_s(T_0) = \frac{\phi_J}{\left(1 - \sqrt{\frac{2T_0}{\epsilon}}\right)^2}. \tag{A3}$$

Thus the increase in packing fraction required to rejam the system at temperature $T_0$ is $\Delta\phi_s(T_0) = \phi_s(T_0) - \phi_J$ [Eq. (8)], which reduces to

$$\Delta\phi_s(T_0) \approx 2\phi_J\sqrt{\frac{2T_0}{\epsilon}} \tag{A4}$$

in the $T_0 \to 0$ limit.

## APPENDIX B: VIBRATIONAL RESPONSE FOR DISORDERED VERSUS CRYSTALLINE PACKINGS

In this Appendix, we show that the vibrational response of positionally ordered systems with purely repulsive contact interactions is similar to that for disordered packings. In Fig. 8, we compare the vibrational response of (a) amorphous and (b) crystalline disk packings. In panel (c), we show that the average number of contacts $\langle N_c\rangle$ (normalized by the value at zero temperature, $N_c^0$) versus the input kinetic energy $T_0$ is similar for both disordered and crystalline packings (at least until cage-breaking particle rearrangements occur). Note that for the simulations of the amorphous packing in Fig. 8(a), we did not remove the floater particles with fewer than three interparticle contacts. We normalized the number of contacts by $N_c^0$ so that we could directly compare the behavior of the contact number for amorphous and crystalline systems. The degree to which positional order affects the nonlinearities from contact breaking is a very interesting question, and this will be investigated in future studies.

## APPENDIX C: SYSTEM SIZE AND CONFIGURATION DEPENDENCE

In this Appendix, we investigate the system-size dependence and configurational fluctuations of the time-averaged contact number $\langle z\rangle$ as a function of the packing fraction deviation $\Delta\phi$ and input kinetic energy $T_0$. As shown in Fig. 1(c), the system-size dependence of $\langle z\rangle/z_{\rm iso}$ is weak for $T_0$ below the temperature $T_{cb}$ at which cage-breaking rearrangement events occur. However, for a given system size,

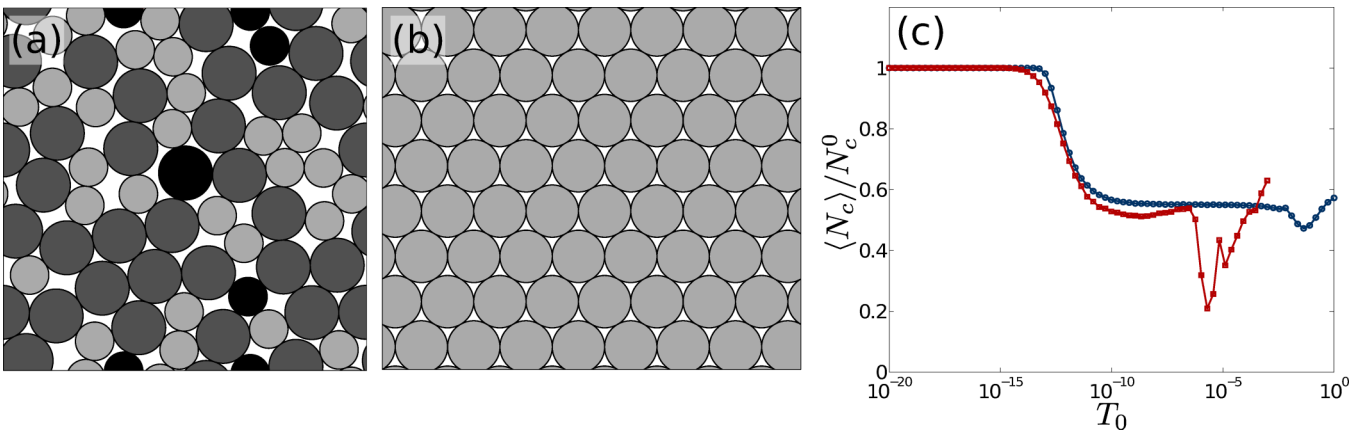


FIG. 8. (Color online) (a) Disordered packing of $N = 64$ bidisperse disks in a square periodic cell. Half of the disks are large with diameter $\sigma_2 = 1.4\sigma_1$. The "floater" disks with fewer than three interparticle contacts are shaded in black. (b) Packing of $N = 64$ monodisperse disks on a triangular lattice in a rectangular periodic cell with dimensions $1\times\sqrt{3}/2$. (c) Average number of interparticle contacts $\langle N_c\rangle$ normalized by the number $N_c^0$ at $T_0 = 0$ as a function of the input kinetic energy $T_0$ for the disordered packing (squares) in (a) and the crystalline packing (circles) in (b) at $\Delta\phi = 10^{-6}$.

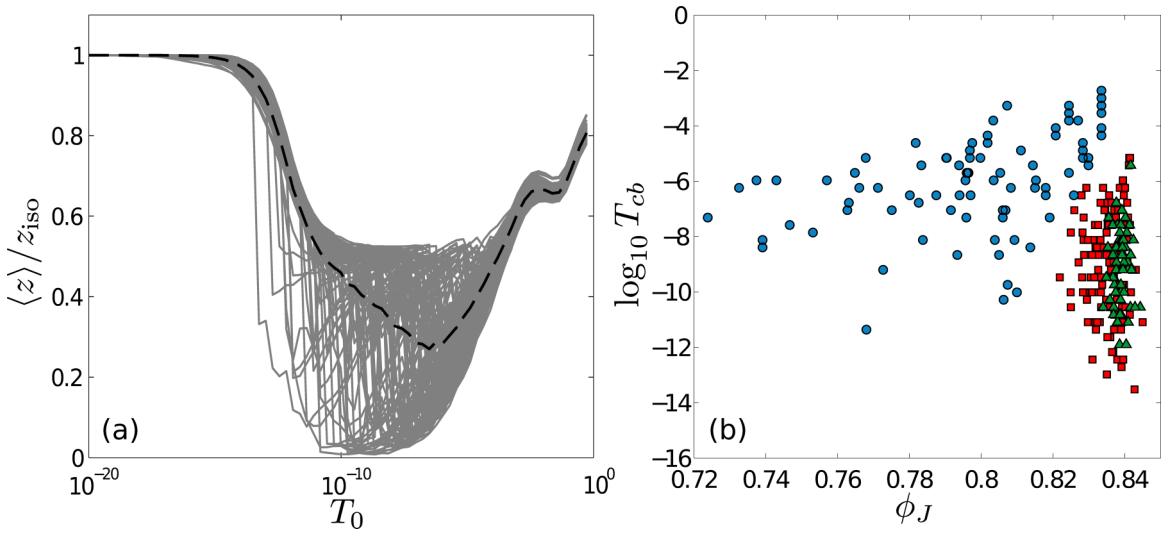


FIG. 9. (Color online) (a) Normalized contact number $\langle z \rangle / z_{\rm iso}$ versus input kinetic energy $T_0$ for 100 different packings (gray lines) with $N = 128$ and $\Delta\phi = 10^{-6}$. The sudden drop in contact number for a given packing indicates a particle rearrangement event. The dashed line gives the average of $\langle z \rangle / z_{\rm iso}$ over the 100 packings. (b) Temperature $T_{cb}$ at which a rearrangement event occurs for each of the 100 packings for $N = 10$ (circles), 128 (squares), and 512 (triangles) at $\Delta\phi = 10^{-6}$ as a function of the initial jammed packing fraction $\phi_J$.

$T_{cb}$ fluctuates significantly from one packing to another, as shown in Fig. 9. Even though the distribution of jammed packing fractions narrows with increasing system size [25], we do not find a significant narrowing of the distribution of $T_{cb}$ in the large-$N$ limit.

In Fig. 10, we show that the "phase diagram" for the vibrational response for a $N = 128$ MS packing is qualitatively similar to that for an $N = 10$ MS packing (cf. Fig. 1 in the main text). The boundary for single contact breaking $\phi_c(T_0)$ shifts to lower $T_0$ and larger $\Delta\phi$ with increasing $N$, which indicates that the transition region between the ICS and HCS grows with system size. This feature is highlighted in Fig. 11, where we show that the width of the transition region in $\langle z \rangle(T_0)$ above jamming increases with system size. The fact that the HCS regime is smaller for the $N = 128$ packing compared to the $N = 10$ packing is mainly a reflection of the large configuration-to-configuration fluctuations of $T_{cb}$, as shown in Fig. 9(b). The particular $N = 128$ packing shown in Fig. 10 rearranges at a smaller $T_{cb}$ than that for the $N = 10$ packing in Fig. 1(a). Note that the configurational average of $\langle z \rangle(T_0)$ differs significantly from $\langle z \rangle(T_0)$ for any single MS packing [Fig. 9(b)]. We deliberately do not average $\langle z \rangle / z_{\rm iso}$ over MS packings [e.g. in Fig. 1(c)], so that we do not obscure the plateau behavior of each single MS packing.

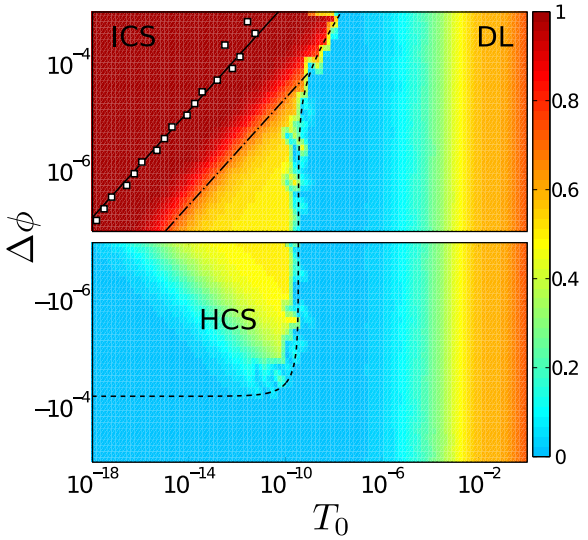


FIG. 10. (Color online) Phase diagram for the vibrational response in the $\Delta\phi$ and $T_0$ plane for a $N = 128$ MS packing with a typical cage-breaking rearrangement temperature $T_{cb}$, where the shading indicates the time-averaged contact number $\langle z \rangle / z_{\rm iso}$ normalized by the isostatic value. The line types and symbols are the same as in Fig. 1.

Cage-breaking particle rearrangements induce changes in the packing fraction at jamming onset $\phi_J$, i.e., the nearest MS packings to energy-minimized configurations for $\Delta\phi < \Delta\phi_{cb}(T_0)$, are different than the reference MS packing. The change in the reference MS packing gives rise to the decrease in the time-averaged contact number to $\langle z \rangle \sim 0$ for $T \gtrsim 10^{-10}$ above the cage-breaking rearrangement boundary in Fig. 10. Note that $\langle z \rangle$ does not drop to zero for all MS packings, but it does drop to zero for *most* MS packings, with an average minimum value $\langle z \rangle_{\rm min} \approx 0.24 \pm 0.15$ for $N = 128$. In future studies, we will determine the vibrational response in glassy systems as a function of the number and types of rearrangement events that occur.

## APPENDIX D: DISCRETE PEAKS IN THE DENSITY OF VIBRATIONAL FREQUENCIES

In this Appendix, we study the resolution of the $2N - 2$ nontrivial, discrete peaks in the density of vibrational frequencies $D(\omega^v)$ from the Fourier transform of the velocity autocorrelation function in the ICS (Fig. 2) as a function of the temporal resolution of the time series for the particle velocities.

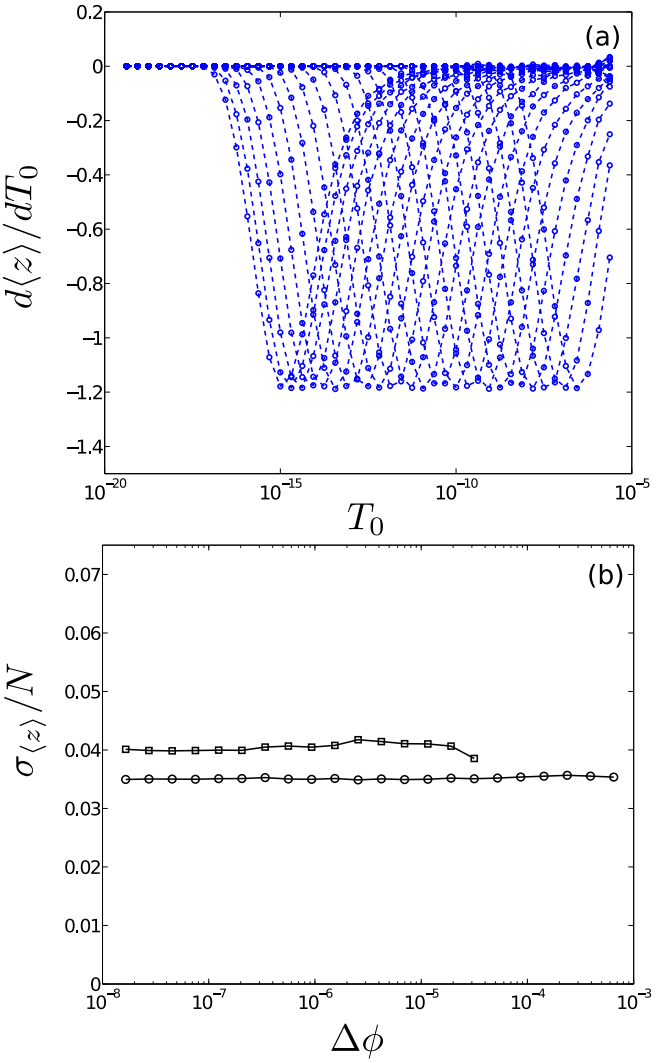


FIG. 11. (Color online) (a) Slope of the time-averaged number of contacts as a function of $T_0$ for a typical $N = 10$ packing compressed to a set of logarithmically spaced $\Delta\phi$ above jamming onset. (b) Width of the slope in (a) scaled by $N$ for typical $N = 10$ (circles) and 128 (squares) packings compressed to $\Delta\phi$ above jamming.

From Eq. (3), the velocity of particle $n$ in a strictly harmonic system is

$$v_n(t) = \sum_{k=1}^{2N} A_k \omega_k^d e_n^k \cos\left(\omega_k^d t + \psi_k\right), \tag{D1}$$

where $\omega_k^d$ are the eigenfrequencies and $e_n^k$ are the eigenvectors of the dynamical matrix. $A_k$ and $\psi_k$ are determined by the $4N$ initial positions and velocities. For our initial conditions, $\psi_k = 0$ and $A_k = (2/\omega_k^d)\sum_{n=1}^{2N} v_n(0)(e_n^k)^{-1}$. The discrete density of vibrational frequencies $D_l = D(2\pi l/\Delta M)$ is obtained from the discrete fast-Fourier transform of the velocity autocorrelation function using $M$ sampled points of the integrated velocities $v_{nm} = v_n(m\Delta)$, where the total sample time $\Delta = 100\Delta t$ and $\Delta t$ is the integration time step. Then,

$$D_l = \frac{1}{2N}\sum_{n=1}^{2N}\sum_{m=\frac{M}{2}}^{\frac{M}{2}-1}\sum_{k=\frac{M}{2}}^{\frac{M}{2}-1} v_{nm} v_{nk} e^{-2\pi i l(m-k)/M}. \tag{D2}$$

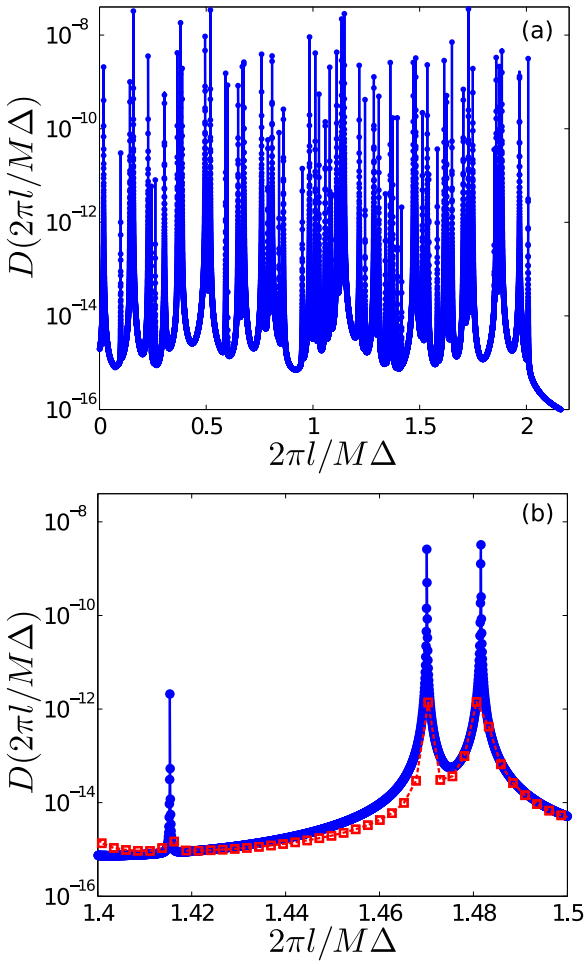


FIG. 12. (Color online) (a) Comparison of the discrete Fourier transform of the velocity autocorrelation function using $M = 1.22\times10^5$ (blue circles) with the theoretical prediction [Eq. (D3), blue solid line] evaluated at the same frequencies for a typical $N = 32$ packing compressed to $\Delta\phi = 10^{-6}$. (b) Same as panel (a) for two sampling times, $M = 1.22\times10^5$ (blue circles) and $2.44\times10^4$ (red squares), but we instead focus on a narrow range of frequencies. The theoretical predictions for $M = 1.22\times10^5$ and $2.44\times10^4$ are denoted by solid and dashed lines, respectively.

Using Eq. (D1), this triple sum can be reduced to

$$D_l = \frac{1}{4N}\sum_{n=1}^{2N} A_n^2(\omega_n^d)^2\left[\frac{\sin\left[M\left(\frac{\pi l}{M}\pm\frac{\omega_n^d\Delta}{2}\right)\right]}{\sin\left(\frac{\pi l}{M}\pm\frac{\omega_n^d\Delta}{2}\right)}\right]^2. \tag{D3}$$

In Fig. 12, we compare Eq. (D3) with $D_l$ obtained from a $N = 32$ packing undergoing vibrations in the ICS regime for two different sampling times, $M = 1.22\times10^5$ and $M = 2.44\times10^4$, corresponding to 190 and 7.6 times the longest eigenperiod. For both sampling times, we find that Eq. (D3) matches the simulation data exactly, which indicates that the nonzero widths of the peaks in $D(\omega^v)$ in the ICS are due entirely to finite sampling time and not to intrinsic nonlinearities.

[1] E. W. Montroll, J. Chem. Phys. **10**, 218 (1942).
[2] K. N. Pathak, Phys. Rev. **139**, A1569 (1965).
[3] C. Brito, O. Dauchot, G. Biroli, and J.-P. Bouchaud, Soft Matter **6**, 3013 (2010).
[4] K. Chen, W. G. Ellenbroek, Z. Zhang, D. T. N. Chen, P. J. Yunker, S. Henkes, C. Brito, O. Dauchot, W. van Saarloos, A. J. Liu, and A. G. Yodh, Phys. Rev. Lett. **105**, 025501 (2010).
[5] C. F. Schreck, T. Bertrand, C. S. O'Hern, and M. D. Shattuck, Phys. Rev. Lett. **107**, 078301 (2011).
[6] C. F. Schreck, C. S. O'Hern, and M. D. Shattuck, Granular Matter **16**, 209 (2014).
[7] C. P. Goodrich, A. J. Liu, and S. R. Nagel, Phys. Rev. Lett. **112**, 049801 (2014).
[8] In systems where the definition of the diameter of the particle is ambiguous (unlike in particulate systems such as dry granular media), we can define a "long-range potential" to be one where the pair potential extends beyond the maximum nearest Delaunay neighbor distance.
[9] To support this statement, we have studied vibrations in systems composed of frictionless disks that interact via single- and double-sided linear [5] and Hertzian [6] spring interactions. We note that another study [7] presents an alternate point of view concerning the features of the interaction potential that give rise to strong nonlinearities in particulate systems.
[10] A. J. Liu and S. R. Nagel, Ann. Rev. Condens. Matter Phys. **1**, 347 (2010).
[11] M. van Hecke, J. Phys.: Condens. Matter **22**, 033101 (2010).
[12] C. Brito and M. Wyart, J. Chem. Phys. **131**, 024504 (2009).
[13] G.-J. Gao, J. Blawzdziewicz, and C. S. O'Hern, Phys. Rev. E **74**, 061304 (2006).
[14] The vibrational response in HCS is not sensitive to the perturbation method. In systems where particle contacts break continually, the vibrational response is given by a wide, continuous distribution of frequencies [5].
[15] A. Tanguy, J. P. Wittmer, F. Leonforte, and J.-L. Barrat, Phys. Rev. B **66**, 174205 (2002).
[16] A. Ikeda, L. Berthier, and G. Biroli, J. Chem. Phys. **138**, 12A507 (2013).
[17] S. Henkes, C. Brito, and O. Dauchot, Soft Matter **8**, 6092 (2012).
[18] G.-J. Gao, J. Blawzdziewicz, C. S. O'Hern, and M. D. Shattuck, Phys. Rev. E **80**, 061304 (2009).
[19] If we include rattler particles in the packings, systems at $\Delta\phi > 0$ would possess a mixed response with those frequencies $\omega_k^s$ associated with rattlers increasing from zero, whereas all others decrease from $\omega_k^d$ for $T_0 > 0$.
[20] M. Schmiedeberg, T. K. Haxton, S. R. Nagel, and A. J. Liu, Europhys. Lett. **96**, 36010 (2011).
[21] L. Wang and N. Xu, Soft Matter **9**, 2475 (2013).
[22] N. Xu, T. K. Haxton, A. J. Liu, and S. R. Nagel, Phys. Rev. Lett. **103**, 245701 (2009).
[23] C.-J. Hsu, D. L. Johnson, R. A. Ingale, J. J. Valenza, N. Gland, and H. A. Makse, Phys. Rev. Lett. **102**, 058001 (2009).
[24] V. Vitelli, N. Xu, M. Wyart, A. J. Liu, and S. R. Nagel, Phys. Rev. E **81**, 021301 (2010).
[25] N. Xu, J. Blawzdziewicz, and C. S. O'Hern, Phys. Rev. E **71**, 061306 (2005).